Retarding field analyzer for the Wendelstein 7-X boundary plasma

M. Henkel[1], Y. Li[*1,2], Y. Liang[*1], P. Drews[1], A. Knieps[1], C. Killer[3], D. Nicolai[1], D. Höschen[1], J. Geiger[3], C. Xiao[2,4], N. Sandri[1], G. Satheeswaran[1], S. Liu[2], O.Grulke[3], M. Jakubowski[3], S. Brezinsek[1], M. Otte[3], O. Neubauer[1], B. Schweer[1], G. Xu[2], J. Cai[2], and the W7-X team[3,a]

[1]Forschungszentrum Jülich GmbH, Institut für Energie- und Klimaforschung – Plasmaphysik, Partner of the Trilateral Euregio Cluster (TEC), 52425 Jülich, Germany
[2]Institute of Plasma Physics, Chinese Academy of Sciences, Hefei 230031, China
[3]Max-Planck-Institut für Plasmaphysik, Greifswald, Germany
[4]Department of Physics and Engineering Physics, University of Saskatchewan, 116 Science Place, Saskatoon, SK S7N 5E2, Canada

A bi-directional multi-channel retarding field analyzer (RFA) probe has been successfully developed for the first time on the Wendelstein 7-X (W7-X) stellarator boundary plasma. Modifications to the RFA prototype hardware and its upgrade for the two W7-X island divertor campaigns are presented, including the electronics. In this paper the experiences and challenges operation and customizing an RFA at W7-X are discussed, as well as the data analysis using a maximum coefficient of determination method to obtain the ion temperature based on the measured modulated ion current. Edge ion temperature profiles have been measured in the standard and high iota configurations.

Keywords: retarding field analyzer, ion temperature, stellarator, Wendelstein 7-X, island divertor.

1. Introduction

Edge ion temperatures (T_i) in magnetic fusion test devices are rarely measured but yet are important for understanding edge plasma physics, especially the thermal equipartition. Currently, routinely operated spectroscopic observations cannot directly measure the fuel ion T_i since the hydrogenic ions do not emit photons. And the low temporal and spatial resolution also limit its function. The alternative Ion Sensitive Probe (ISP) technique is in principle able to measure ion temperatures but suffers from space charge limitation problems in practical applications.[1] The Retarding Field Analyzer (RFA) remains a practical tool to measure the edge ion temperature. To date, RFAs have been used on JET[2, 3], Tore Supra[4], Alcator C-mod[5], ISTTOK[6], STOR-M[7], and EAST[8] tokamaks and other plasma devices to measure the edge ion temperature profile. However there are few reports [9] on the RFA hardware and operation in the stellarator devices where some issues due to 3D magnetic configuration may only been encountered in addition to those found in tokamaks. This paper presents a RFA development for the Wendelstein 7-X (W7-X) device based on the prototype of a multi-channel probe head first tested at EAST [10].

Generally, a RFA consists of one entrance slit to repel the thermal electrons, two or three grids to retard low energy ions and to prevent secondary electron emission, and one collector to measure the ion flux through the grids. The probe can measure the distribution of the charged particle velocity along the direction parallel to the magnetic field, $f(v_\parallel)$, based on the dependence of the collector current on the repelling voltage applied to the grid, or the commonly termed I-V characteristics. The I-V curve is then fitted to an exponential function to extract the ion temperature if a Maxwellian velocity distribution is assumed.

This paper focuses on the hardware and operation of a bi-directional RFA in W7-X, and presents measured data process. Section 2 describes the design and operation of the RFA probe. In Section 3 the measurements and their interpretation using a maximum coefficient of determination method are presented. Section 4 summarizes the paper.

2. RFA for W7-X

W7-X is an optimized stellarator with great flexible magnetic configurations, including different edge island configurations with the island mode number n/m=5/4, 5/5, 5/6.[11, 12] The objective of W7-X is to demonstrate quasi-steady state operation with plasma parameters, including ion temperatures, close to those of a future fusion power plant. It has a plasma volume ~30m^3, major radius ~ 5.5 m and effective minor radius ~0.55 m. The edge plasma parameters, plasma density and temperature near the separatrix n_{es} and T_{es}, are roughly $n_{es}<3\times10^{19}$ m^{-3}, $T_{es}<100$ eV during experimental operation[13]. The corresponding high power fluxes of the W7-X boundary plasma necessitates the RFA to be mounted onto a multiple-purpose manipulator [14, 15] (MPM) shaft to be first slowly moved to the parking position and then quickly inserted into the plasma with a maximum plunge distance of 35 cm, a maximum acceleration of 30 m s^{-2}, and a maximum speed of 2.5 m s^{-1}. The MPM is located in the outer mid-plane with $Z = -171$ mm and toroidal angle φ=-159.26°, in between the characteristic bean shaped and triangular cross section.[14] A variety of diagnostic probes [16-18] mounted on the MPM have been developed for the measurements of edge profiles like the edge electron temperature and density, and plasma flow. An RFA prototype for W7-X was first tested on

*author's email: y.li@fz-juelich.de and y.liang@fz-juelich.de
[a]See the author list in T. Klinger et al., Nucl. Fusion 59 112004 (2019).

EAST[10] and then upgraded in the first divertor operation campaign of W7-X in 2017. However due to several problems encountered in the first campaign, the RFA probe mechanical structure and electronics were significantly upgraded for the 2018 campaign. This paper discusses the development of the RFA beyond what was employed in EAST, and data subsequently measured successfully in W7-X. Issues overcome during RFA operation on W7-X are discussed in detail in sub-section 2.3.

2.1 RFA body design

Figure 1 shows the design of a bi-directional 3-channel-array RFA head used for the W7-X. To match the bean-like magnetic geometry of W7-X, the RFA head has been rotated 18 degrees upwards in the poloidal direction compared to the original device used in EAST. The probe body consists of two identical analyzers mounted back to back. As shown in Fig. 1, the analyzer on each side contains a 3-mm thick tungsten entrance orifice plate (white color sheet), a newly installed thin tungsten entrance slit plate with a thickness of 50 µm, three successive grids (green color sheets), and three collector plates (white, blue and purple color sheets). The physical and electrical separation between the adjacent grid sheets is maintained by a ceramic spacer plate (orange color sheets) with a thickness of 1 mm.

Instead of the sheet previously employed with a vertical slit array using a spacer width of ~ 100 µm in the W7-X 2017 campaign, the thin entrance slit plate (thickness ~50 µm) has three, slits openings with a width of ~30 µm and spacing between the slits is 4mm. The compact design allows T_i measurement at three radial locations simultaneously. The slit aperture has to repel the thermal electrons, which requires the width to be smaller than the Debye length ($\lambda_D = \sqrt{\varepsilon_0 k_B T_e / n_e e^2}$), where ε_0 the vacuum permittivity, k_B the Boltzmann constant, T_e electron temperature, n_e the electron density, and e the elementary charge). λ_D is in the range 5-50 µm in the W7-X scape-off layer (SOL). The actual slit width of ~25µm has been verified by a microscope (as shown in Fig. 2). To prevent high heat load plasma impinging on the thin entrance slit plate, the thick entrance orifices originally designed in EAST have been reversed to attach with the thin entrance plate. The front tungsten plate is cut with three trapezoid orifices to enhance the input ion flux. The angle between the lateral sides is 45°. The short base width of the trapezoid slit is ~300 µm. The thick plate is made by wire eroding and the thin entrance slits are cut by laser. Each grid is made out of a flat tungsten blank (thickness ~50 µm) on which a regular two dimensional array of square openings is machined. As in the original design, the sides of the square opening is 0.4 mm and the bar width between the opening is 0.1 mm. The optical transmission of the grid is 64%. In the 2018 campaign, the shape of the grid base has been optimized to minimize the surface area in order to decrease the capacitance between the grid and the collector. On the base of the grids and the thin slit plate a small section of grid-style holes has been machined so the 0.3mm diameter copper wires can be crimped to the section to transmit electrical signals.

After the bias voltage is applied to the grids, the ions would first pass through an electrical field changing in time and location inside the RFA cavity. If the ion energy were larger than the maximum potential which generally located at Grid 2 biased with sweeping voltage, ions will reach the collectors and contribute to the total current measured by the external electronic circuits. Each collector fixed at the ceramic base measures the ion current passing through the corresponding entrance slit. The bi-directional RFA components are fastened by two sets of screws and nuts which are electrically insulated with the six grids. The two thick entrance slit plates in both sides are electrically connected with each other and self-biased negatively with respect to the plasma space potential. A boron nitride cover (green color cover in Fig. 1) is chosen to protect the RFA components.

In addition to the RFA components described, there are also five tungsten Langmuir tips and one stainless steel gas inlet (tube inner diameter 2.5mm) at the RFA probe top. These Langmuir probes are 2mm in diameter and 3mm long over the outer cover of the boron nitride cover. 0.5mm diameter wires are used to connect with the Langmuir tips to the external circuitry. During RFA operation, three of the six channels measure the ion current, demonstrating the soundness of the RFA hardware design and assembly. Only three of total five Langmuir tips are used as a triple probe due to the limitation on the number feedthrough channels on the MPM system.

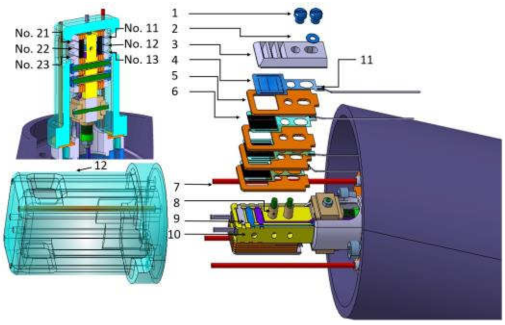

FIG. 1. Sectional and exploded isometric decomposition views of the W7-X multi-channel RFA probe head, which contains 1, screw; 2, gasket; 3, orifice plate; 4, thin entrance slit plate; 5, ceramic spacer plate; 6, grid; 7, Langmuir probe; 8, nut; 9, collector; 10, ceramic base; 11, grid-style holes; 12, boron nitride cover, and the channel number named as No. 11, 12, 13 in one side and No. 21, 22, and 23 in the other side.

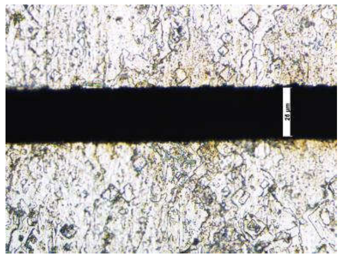

FIG. 2. Thin entrance slit width measured by a microscope

2.2 RFA circuit design

The RFA circuit has been designed to flexibly control and monitor the bias voltages on the entrance slit plates and the grids. An overview of the circuit schematic for RFA measurement is shown in Fig. 3. Most of the corresponding components are connected in parallel into each power supply. However, each of the six RFA channels uses a separate collector plate for independent ion current measurement. The circuit design allows measurement of ion current in a wide range from 1mA to 10A by remotely switching the current sampling shunt resistor in five steps from 100 Ω to 10 mΩ. The bias voltage for the slit plates and six grids are monitored at the points indicated by the red solid dots in Fig. 3 through a circuit with an input resistance of 1MΩ. The power supply parameters can be remotely programmed based on experimental needs. Table 1 lists the biasing supply parameters including their types of waveforms, adjustable voltage range, and maximum current. Figure 3 also shows the triple probe circuit. The circuit ground is connected to the W7-X vessel ground. The current and voltage signals are measured via optoelectronic isolators by the data acquisition (DAQ) system.

During the RFA operations, the RFA circuit has been operated with two floating entrance slits to protect the wires from possible transient high current. Grids 1 and 3 are biased by a negative DC voltage, -100 V and -200 V, respectively. Grid 2 is biased by a sweep voltage supply at an adjustable programming frequency.

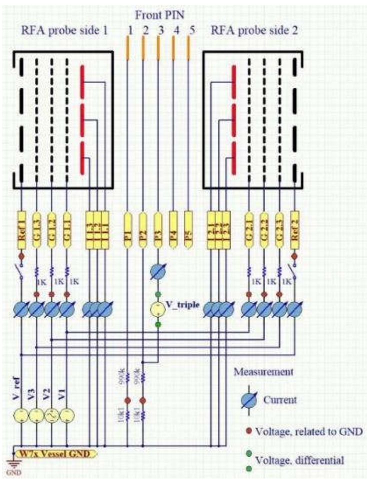

FIG. 3. The RFA circuit sketch, where Pins 1, 2 and 3 are used to measure the plasma floating potential, positive potential, and ion saturated current, respectively.

TABLE I. RFA electronic scheme.

System	*Type*	*Voltage range (V)*	*Max current (A)*
V_{ref}	DC	0 - 160	10
V_1	DC	0 - 320	10
V_2	AC +DC offset	AC: ±300, max 10kHz DC: ±200	2 1
V_3	DC	0 - 160	10
V_{triple}	DC	0 - 320	10

2.3 RFA operation in W7-X

Operation of the RFA as described has been performed in the two first divertor operation campaigns of W7-X in 2017 and 2018, encountering challenges in both campaigns which needed to be overcome. Firstly, during the 2017 RFA operation, the RFA grid sheets were destroyed as shown in Fig. 4. The wires connecting the grids were also broken. The damage pattern points to arcing between the grids as most likely mechanism. To solve these issue, a 1 kΩ high power resistor was added to the six-grid circuits to reduce the current flowing through the grids, as shown in Fig. 3. The carbon cover originally designed to be floating was anomalously biased with a large -190V DC voltage which may have been caused by the broken wires. To avoid this, the carbon cover was replaced with one made of boron nitride. In addition, operation of the RFA was conducted in a more conservative manner in the 2018 campaign. All the grids during the first plunge of the RFA were without the bias voltage to clean the RFA cavity by hot plasma. Following initial exposure, the biased DC and AC powers were imposed on the grids in a stepwise, incremental manner in subsequent discharges.

Secondly, plasma conditions in W7-X have been observed to affect the measurements of RFA adversely in ways not experienced on EAST. Usually in W7-X, potential in the SOL is strongly positive in the low plasma density regime [19]. Because the RFA entrance slit is floating, its potential could exceed the sweeping voltage on Grid 2. Under these conditions, the ion influx inside the RFA cavity then would not be modulated by the sweeping voltage. The collected current on the collect tends to saturation. A typical example is shown in Fig. 5. In this discharge #180816021, the ECRH heating power is 2 MW and the center line integrated plasma density is nearly constant, $\sim 2.5\times10^{19}m^{-2}$, controlled by gas puffing. The magnetic configuration is EIM+252,[20] meaning the standard configuration with a field strength of 2.52 T at phi=0° (ECRH-launching plane) at the magnetic axis. The floating potential measured by the entrance slit gradually increases as the probe moves to the separatrix. Larger voltage on the entrance slit leads to smaller modulating ion flux range. Care should be taken to compare the measured floating potentials from the Langmuir probes to the biasing applied the RFA grids to preselect faulty. To measure the modulated ion current in the current setup, the RFA experiment has to been limited in the high plasma density regime, i.e., $n_{el}>7\times10^{19}m^{-2}$.

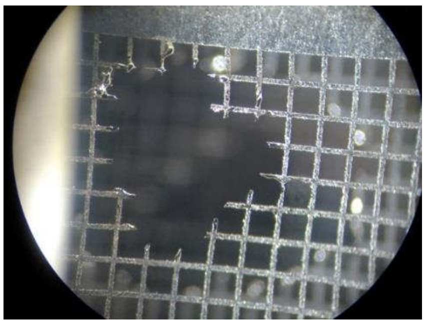

FIG. 4. Photo of the damaged RFA grids during the first island divertor campaign.

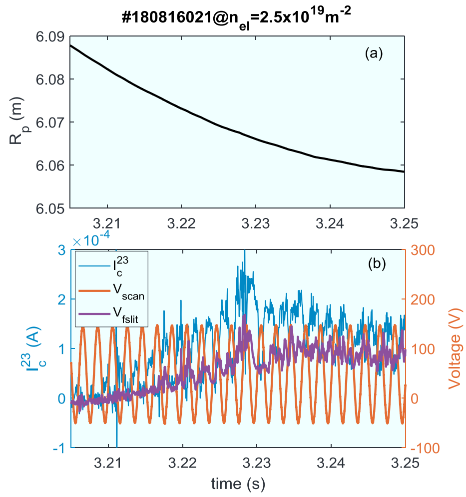

FIG. 5. Evolution of (a) major radial position and (b) modulated ion currents of channel 23, scan voltage, and floating potential on the entrance slit.

3. Ion temperature measurement

3.1 Ion temperature interpretation

The measured RFA current can be expressed by the following formula, assuming that the fuel ions of charge eZi dominate the incident ion flux,

$$I_C = A_{beam} e Z_i \int_{\sqrt{2eZ(V_2 - V_S)/m_i}}^{\infty} \xi_{total} v_{||} f(v_{||}) dv_{||} \quad (1)$$

where I_C is the RFA collector current, Abeam the ion beam area, e the electron charge, mi the ion mass, Z_i the ion charge number, V_2 the retarding sweep voltage, V_s the sheath potential, ξ_{total} the total ion transmission coefficient, $f(v_{||})$ the ion distribution function for the velocity component parallel to the magnetic field line. Assuming that the ion velocity distribution function in the unperturbed plasma near the RFA probe is Maxwellian, Eq.1 can be simplified to

$$I_C = \begin{cases} I_0, & V_2 < V_s \\ I_0 e^{-(V_2 - V_S)Z/T_i}, & V_2 \geq V_s \end{cases} \quad (2)$$

where I_0 is the maximum ion current when no ions are repelled by the retarding potential V_2.

During operation of the RFA, three collector channels (channel numbers 11, 12 and 23) measure modulated ion currents as the voltage applied to Grid 2 is scanned from -20 V to 200 V. Since the modulated signal is weak and submerged in noise including the plasma fluctuation, an auto-correlation power spectral densities were calculated to extract the modulated signals. The result is shown in Fig. 6, where the power spectral density for each channel has been calculated in the before (dash line) and after (solid line) entering plasma phases. In this discharge #180905020, the main plasma is confined by the standard configuration and maintained by 3MW X2 heated electron cyclotron resonance heating (ECRH) power. A nearly constant central line integrated electron density n_{el}= 7×10^{19}m^{-2} is controlled by gas puffing. The RFA was plunged into the plasma at 5.2 s. Before the probe enters the plasma, these three channels can only measure the background noise and show similar noise spectrum with dominant noise frequency primarily above 80 kHz. After the probe reaches the SOL in close proximity to the separatrix, the plasma turbulence becomes prominent near frequency ~200 kHz and enhance larger fluctuation for higher frequency (>10kHz) in channels 11 and 12 than in channel 23 even though all channels are designed to behave identically. The reason for this phenomenon is still unclear. In this case, to obtain clear modulated currents for I-V curve fitting, the collector currents were first low-pass filtered with a cutoff frequency 10 kHz for channels 11 and 12, and 30 kHz for channel 23. They were then subtracted by the induced current due to the inductive coupling between Grid 2 and the collector. Figure 7 shows the waveforms of the collector currents and scan voltage as the probe moves over a distance of ~1cm into the plasma. After the smoothing process, a clear modulated current has been observed in channel 23, while the collector currents on channels 11 and 12 still contain a certain amount of noise which contributes to variability in the modulated current.

The ion temperature is obtained by fitting the I_c-V_2 curve based on Eq. (2) and assuming Z = 1 (hydrogen plasma). Since the initial input setting could affect the fitting result, the initial parameters in Eq. (2) have been scanned, named as T_i^{scan} and V_s^{scan}, to obtain the best fitting curve with a maximum coefficient of determination R^2, which is assumed to be closest to the plasma parameters. The output parameters of the fitting curve, named as T_i^{fit} and V_s^{fit} would also change with different initial parameters. The results of R2 and the corresponding T_i^{fit} as functions of the scanned T_i^{scan} and V_s^{scan} are shown in Fig. 8(a), where the experimental data used for fitting is from channel 11 and within the time interval [5.246 5.248]s for two scan periods as shown in the rectangular shaded area of Fig. 7. The maximum R^2 point is expressed by a red circle. As can be seen in this figure, T_i^{fit} gradually decreased from 80 to 60 eV and kept almost constant as increasing the input parameters of T_i^{scan} and V_s^{scan}. The fitting counts of T_i^{fit} and V_s^{fit} displayed as a histogram in Fig. 8(b) shows that the maximum R^2 points (red circle) is located near the largest number of areas. This indicates that the maximum R^2 points coincide with the most probable point. After obtaining the parameters of T_i^{fit} and V_s^{fit} with maximum R^2, the I_c-V_2 curve fitting of three channels are plotted in Fig. 9. The fitting curve parameters of T_i and V_s are also shown in this figure. Note that the measurement radial position is still ~2 cm away from the separatrix (R_{sep}≈6.04 m). Since the I_c signals of channels 11 and 12 have much larger noise comparing with channel 23 as shown in Fig. 7, the I_c-V_2 data shows much clearer exponential trend for channel 23 than in channels 11 and 12. As a consequence, the fitting uncertainty is much larger in channels 11 and 12 than in channel 23.

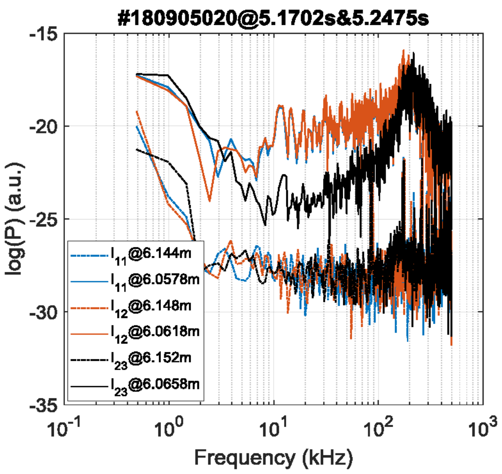

FIG. 6. The auto-correlation power spectral density of collector currents measured by channel 11, 12 and 23. Data are shown before (dashed lines) and after (solid lines) entering the plasma.

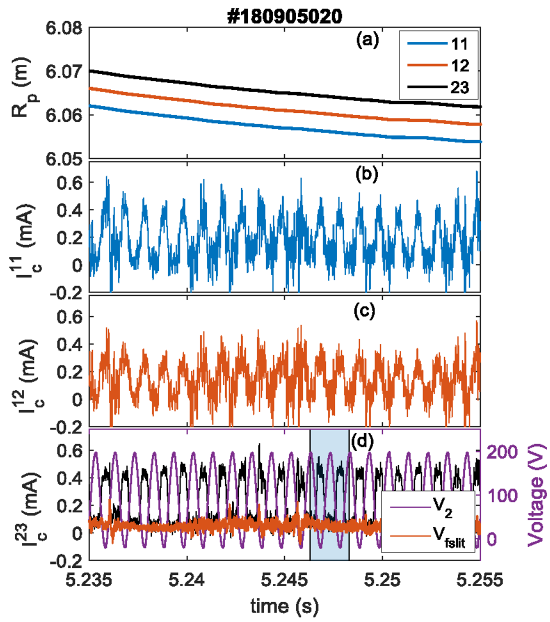

FIG. 7 Evolution of (a) major radial position and modulated ion currents of the channel 11 (b), 12 (c) and 23 (d). Note that the cutoff frequency are 10 kHz in channel 11 and 12, and 30 kHz in channel 23.

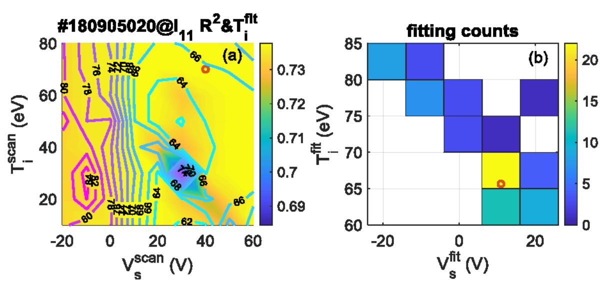

FIG. 8 (a) R^2 and the corresponding T_i^{fit} as functions of the scanned T_i^{scan} and V_s^{scan}; (b) fitting counts of T_i^{fit} and V_s^{fit}. The maximum R^2 is covered as red circle. The time interval corresponds to the shaded span as shown in Fig. 7.

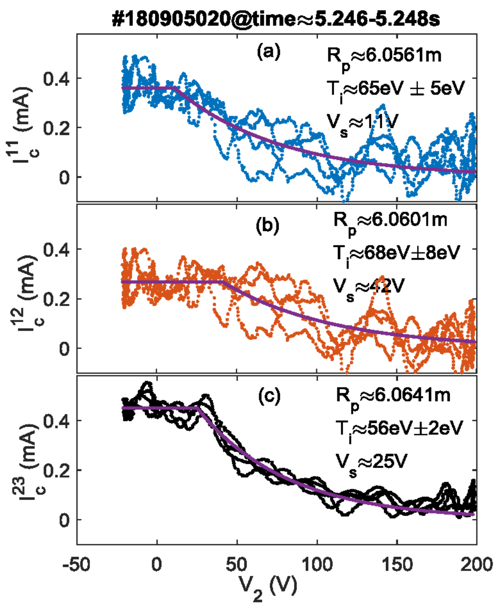

FIG. 9 Example RFA characteristics and fitting curve and results for channel (a) 11, (b) 12, and (c) 23. The time interval corresponds to the shaded span as shown in the lowest panel in Fig. 7.

3.2 Ion temperature profile at the W7-X plasma boundary

The retarding field analyzer was installed on the MPM during programs with the high iota and standard configuration in the 2018 campaign. In Fig. 10 the field line connection length distribution and Poincare map for this plasma shape are shown, overlaid with the probe movement trace. In the high iota configuration (FTM+252), panel (a)-left, the formed 5/4 edge island chain shifts both the separatrix and the SOL region inward compared with the standard configuration (EIM+252), panel (b)-right, which forms a 5/5 island chain in the plasma boundary. The major radius of the separatrix at the RFA movement Z position has been shifted inwards from Rsep≈6.04m, with the standard configuration, to 6.01m, with the high iota configuration. The radial width of the edge island in the high iota configuration is also much smaller than in the standard case. The fitted ion temperature profiles, in channels 11, 12 and 23 are shown in Fig. 11, where only the maximum coefficient of determination R^2 larger than 0.7 is displayed. The connection length profile along the probe movement path are also covered into the figure. The plasma in the FTM configuration is operated at 2 MW O2 heated ECRH power and n_{el} =9×10^{19}m^{-2}. Since heating power is lower and plasma density is higher, the observation of lower ion temperature is expected in FTM compared to the EIM configuration, as shown in Fig. 11. Because of the island configuration effect, the edge ion temperature profile has been observed to move further inwards when the configuration is changed from standard to high iota configuration. This profile shift is consistent with the connection length distribution. The ion temperature profile seems expanded and flattened by the larger island geometry in the standard configuration. The FLUX probe also measures plasma electron temperature and density profiles are much broader in standard configuration than in others [13].

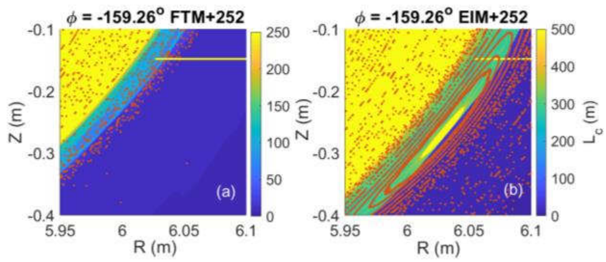

FIG. 10. Connection lengths profiles and superimposed magnetic configuration in (a) high iota configuration, FTM+252 and (b) standard configuration, EIM+252, where the color code is connection length, red dots are Poincare plot and yellow lines shown the MPM path.

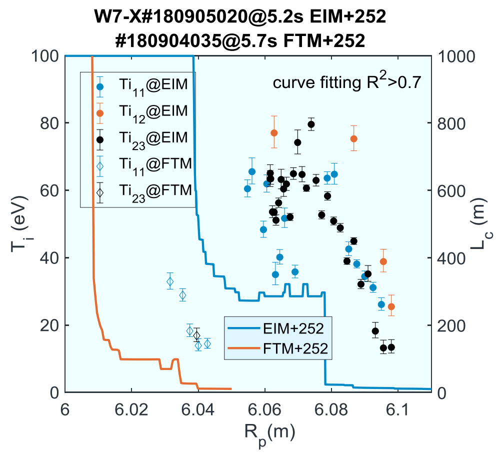

FIG. 11. Ion temperature profiles in high iota (Rp=6.032-6.043 m) and standard configuration (Rp=6.055-6.1 m) measured from channels 11, 12, and 23. The error bar of Ti represents the confidence interval of fit. The coefficient of determination, denoted R2, is >0.7.

4. Summary

A retarding field analyzer probe has been successfully developed for the first time for the W7-X stellarator boundary plasma. This work presents challenges in adaptation of the RFA design to a stellarator, with significant results showing ion temperature in multiple configurations of W7-X for the first time. The RFA probe consists of a front plate with 3 entrance orifices (width 300 µm, length 8 mm per orifice) on top of a newly added thin plate with 3 narrow entrance slits (width 30 µm, length 8 mm per slit and thickness 50 µm) aligned and in electrical contact with the front plate, three successive grids, and three separate collector plates. The RFA circuit is designed to flexibly control and monitor the bias voltages on the entrance slit plates and the grids. Specific challenges that were overcome related to T_i in the 2017 campaign include the following: the RFA hardware has been upgraded with respect to both the probe mechanical structure and the electronics. The carbon cover of the probe was replaced by a boron nitride cover. Two Langmuir pins in the previous design have been extended to five pins on the top of the RFA probe to simultaneously measure the electron density, electron temperature and the turbulence information. The sampling circuits of all the grids were also upgraded to prevent the damage caused by arcing between the grids. To avoid large positive floating potential in the W7-X SOL, the probe has been limited to be operated in high density discharges (n_{el}>7×10^{19}m^{-2}). The ion temperature has been interpreted by utilizing a maximum coefficient of determination method. The edge ion temperature profile has been observed to be shifted inwards in high iota configuration comparing with the standard configuration.

Acknowledgments

The authors deeply appreciate the continued research and operational efforts of the entire W7-X team. This work has been carried out within the framework of the EUROfusion Consortium, has received funding from the Euratom research and training programme 2014-2018 and 2019-2020 under grant agreement No 633053, and was supported by the International Postdoctoral Exchange Fellowship Program Nos. 20170009, the National Natural Science Foundation of China under Grant Nos. 11705237.

References

[1] D. Brunner, et al., Space-charge limits of ion sensitive probes, Plasma Phys. Control. Fusion, 55 (2013) 125004.

[2] H.Y. Guo, et al., Ion temperature measurements in JET boundary plasmas using a retarding field analyser, Contrib. Plasma Phys., 36 (1996) 81-86.

[3] R.A. Pitts, et al., Retarding field energy analyzer for the JET plasma boundary, Rev. Sci. Instrum., 74 (2003) 4644-4657.

[4] M. Kočan, et al., On the reliability of scrape-off layer ion temperature measurements by retarding field analyzers, Rev. Sci. Instrum., 79 (2008) 073502.

[5] D. Brunner, et al., Scanning retarding field analyzer for plasma profile measurements in the boundary of the Alcator C-Mod tokamak, Rev. Sci. Instrum., 84 (2013) 033502.

[6] I.S. Nedzelskiy, et al., Compact retarding field energy analyzer for the tokamak ISTTOK boundary plasma, Rev. Sci. Instrum., 77 (2006).

[7] M. Dreval, et al., Retarding field energy analyzer for the Saskatchewan Torus-Modified plasma boundary, Rev. Sci. Instrum., 80 (2009) 103505.

[8] Y.L. Li, et al., Retarding field analyzer for the EAST plasma boundary, Rev. Sci. Instrum., 87 (2016) 123503.

[9] I.S. Nedzelskiy, et al., Retarding field energy analyzers for ion temperature measurements in the boundary plasmas of the tokamak ISTTOK and TJ-II stellarator, PROBLEMS OF ATOMIC SCIENCE AND TECHNOLOGY 1(2009) 174-176.

[10] M. Henkel, et al., Multi-channel retarding field analyzer for EAST, Plasma Sci. Technol., 20 (2018) 054001.

[11] H. Renner, et al., The capabilities of steady state operation at the stellarator W7-X with emphasis on divertor design, Nucl. Fusion, 40 (2000) 1083.

[12] T. Sunn Pedersen, et al., First divertor physics studies in Wendelstein 7-X, Nucl. Fusion, 59 (2019).

[13] C. Killer, et al., Characterization of the W7-X scrape-off layer using reciprocating probes, Nucl. Fusion, 59 (2019).

[14] D. Nicolai, et al., A multi-purpose manipulator system for W7-X as user facility for plasma edge investigation, Fusion

Eng. Des., 123 (2017) 960-964.

[15] G. Satheeswaran, et al., A PCS7-based control and safety system for operation of the W7-X Multi-Purpose Manipulator facility, Fusion Eng. Des., 123 (2017) 699-702.

[16] Y. Liang, et al., Diagnostic set-up and modelling for investigation of synergy between 3D edge physics and plasma-wall interactions on Wendelstein 7-X, Nucl. Fusion, 57 (2017).

[17] P. Drews, et al., Operation of probe heads on the Multi-Purpose-Manipulator at W7-X in OP 1.2a, Fusion Eng. Des., (2019).

[18] J. Cai, et al., A new multi-channel Mach probe measuring the radial ion flow velocity profile in the boundary plasma of the W7-X stellarator, Rev. Sci. Instrum., 90 (2019) 033502.

[19] S.C. Liu, et al., The effects of magnetic topology on the scrape-off layer turbulence transport in the first divertor plasma operation of Wendelstein 7-X using a new combined probe, Nucl. Fusion, 59 (2019).

[20] E. Strumberger, SOL studies for W7-X based on the island divertor concept, Nucl. Fusion, 36 (1996) 891-908.